Progress in Earth and Planetary Science

RESEARCH ARTICLE Open Access

Variations in extreme wave events near a South Pacific Island under global warming: case study of Tropical Cyclone Tomas

Kenji Taniguchi[1*] and Yoshimitsu Tajima[2]

Abstract

The intensification of tropical cyclones (TCs) and wind-induced ocean waves is expected to be amplified under global warming conditions. In 2010, strong TC Tomas approached the Fiji Islands and caused severe damage. Here, an ensemble simulation technique is combined with a pseudo-global warming (PGW) method to investigate future variations in TCs and wind-induced ocean waves. Ensemble PGW simulations were implemented using the weather research and forecasting (WRF) model with five different future projections. Hindcast and PGW simulations showed similar tracks of Tomas. In four PGW simulations, the central pressures of the simulated TCs decreased. Enhanced near-surface wind was recognized in three PGW simulations around the Fiji main island (Viti Levu). In the other two future simulations, the surface wind speed was weaker than the one in the present climate because of the slight eastward shift in the track and delayed development of the TC. WaveWatchIII (WW3) was applied for offshore wave simulations forced by the wind field obtained by WRF simulation results. In three future simulations, a clear increase in the maximum significant wave height (H_s) was found on the southeastern coast of Viti Levu. One future simulation yielded almost the same offshore wave characteristics as those under the present climate. In another future simulation, the ensemble mean H_s was as high as that in the present climate, but extremely large H_s values were found in several ensemble members. Future simulations using multiple global climate model (GCM) projections showed possible variations in TCs and wind-induced ocean waves which is useful for the risk assessment of various hazards.

Keywords: Tropical cyclone, Climate change, Ocean waves, Numerical simulations, Ensemble simulation, Fiji

Introduction

Ocean surface waves are generated by local surface wind; thus, wave characteristics are highly affected by variations in atmospheric conditions caused by climate change. In the region of tropical cyclones (TCs), typhoons, and hurricanes, extreme ocean waves cause disaster in coastal areas. A large number of studies have reported an increasing number of the most intense cyclones under future global conditions (Knutson et al. 2010; Marciano et al. 2015; Kanada et al. 2017a; Nayak and Takemi 2019, etc.). Projections of the future ocean wave induced by strong storms (TCs, typhoons, and hurricanes) are crucial for assessing the impact of climate change on coastal regions and the development of appropriate adaptation strategies. Several studies have focused on future variations in cyclone-induced ocean waves and storm surges. Tasnim et al. (2015) performed hindcast and future simulations of TC Nargis. The predicted future cyclone was stronger than that in the present climate. Moreover, the predicted surge in the future TC was approximately 3 m higher than that in the hindcast. Nakamura et al. (2016) conducted numerical weather simulations and storm surge simulation of super typhoon Haiyan under the current and global warming climates. The simulation results indicated that typhoon intensity and storm surge will be larger in the future. Appendini et al. (2017) derived information of TCs from reanalysis data and future projections of global climate models (GCMs) and investigated future variations in wave climates. They found increasing significant wave

* Correspondence: taniguti@se.kanazawa-u.ac.jp
[1]Faculty of Geosciences and Civil Engineering, Kanazawa University, Kakuma-machi, Kanazawa, Ishikawa 920-1192, Japan
Full list of author information is available at the end of the article

height in certain areas. Timmermans et al. (2017) investigated future variations in global wind-induced wave climate and showed further increases in extreme wave height in TC regions. However, there was large variation in wave heights; detail assessments for specific region are indispensable. Patricola and Wehner (2018) investigated anthropogenic influence on extreme TCs. They implemented high-resolution numerical simulations of TCs under the current, pre-industrial, and future climate conditions and found that the intensification of future TCs is larger than the change in TCs from the pre-industrial to the current climate.

For future climate assessment, the output of GCMs are used; however, these model predictions do not include ocean waves, and some analysis or numerical simulation is needed to interpret the effects of any projected change in the climate on ocean waves. Moreover, a high spatial resolution is desirable in such projections to assess detailed impacts of changes in the wave climate for specific coastal areas. Statistical projection is one major approach to produce a wave climate projection. There are also numerous estimations of the future wave climate from numerical wave models. Laugel et al. (2014) compared finer resolution wave climates estimated based on either statistical or dynamical downscaling methods. This study found that the results based on the dynamical method showed better predictive skills of the observed wave climates, and the difference in the computed wave climates between the dynamical and statistical methods was more significant under more severe conditions of global warming. The same study also highlighted that statistical methods have disadvantages in the estimation of the tails of the wave probability distributions or extreme cases. Martinez-Asensio et al. (2016) also compared the results of statistical and dynamical downscaling for the North Atlantic wave climate and found that a statistical model based on wind speed yielded results similar to the dynamical downscaling results. The statistical model using climate indices, sea level pressure, and/or pressure gradient, however, did not reproduce the long-term trend found in the dynamical downscaling results. In addition, statistical downscaling methods neglect swell effects (Mori et al. 2013). Therefore, dynamical methods could be more appropriate for estimating the possible impact of climate change under more severe conditions.

Hemer et al. (2013) showed that the direct use of GCM output to force a wave model can cause biases in the wave climate or the overestimation of wave generation in broad regions of the southern Pacific Ocean due to swells. Subsequent work by Hemer and Trenham (2016) showed poorer skill in wave simulation or larger negative biases in the wave height when the GCMs output from the Coupled Model Intercomparison Project Phase 5 (CMIP5; Taylor et al. 2012) was directly used to force a wave model. To prevent the above-referenced bias effects of the GCMs, a pseudo global warming (PGW) method has been proven to be useful (Sato et al. 2007). In early PGW method, atmospheric conditions were generated by considering variations of thermodynamic and momentum conditions under increasing atmospheric temperature (Schär et al. 1996). In the recent PGW method, future anomalies generated from the GCM output are added to the reanalysis data. Then, new future conditions (or PGW conditions) are produced. The PGW conditions are very similar to the reanalysis data used as initial and boundary conditions for reproductive simulations. However, they contain large-scale differences in future climatological conditions. Simulations forced by the PGW conditions can be compared with simulations forced by the reanalysis data, which are expected to be more accurate than the results obtained from the direct use of the GCM outputs. To evaluate possible future variations in extreme weather events, the PGW method was applied to actual past extremes (Hill and Lackmann 2011; Lackmann 2015; Meredith et al. 2015; Taniguchi and Sho 2015).

The South Pacific is one of the major ocean basins where TCs occur. Most tropical islands are affected by the passage of violent storms. At the same time, Fiji is located along the southern border of the South Pacific convergence zone and is exposed to seasonal trade winds that greatly influence the wave climate. In March 2010, TC Tomas hit the northern and eastern areas of Fiji as a Category 4 TC on the Saffir-Simpson scale. Tomas brought destructive winds and heavy rains. In Fiji, two lives were lost, 649 houses were destroyed, and 1387 houses were damaged. The Fiji National Disaster Management Office estimated that the total damage was almost $43.6 million USD. Regarding TC behaviors in the South Pacific, decreasing frequency is reported (Walsh et al. 2012; Bell et al. 2019; Walsh et al. 2015; Zhang and Wang 2017; Yoshida et al. 2017). Walsh et al. (2015) showed insignificant variations in frequency of intense TCs under the global warming condition. Zhang and Wang (2017) found that decreasing tendency is more significant for weak TC in the South Pacific. On the other hand, results in Yoshida et al. (2017) indicates decreasing frequency of category 4 or 5 TCs. These results indicate uncertainty in future variations of TC in the South Pacific.

In this study, numerical weather simulations with the PGW method are implemented for TC Tomas. An ensemble simulation technique (i.e., the lagged-simulated perturbation (LSP) method) developed by Taniguchi (2018) is combined with the PGW simulations to consider uncertainties in the forcing data of the simulations. Then, wave simulations are determined with wind data

from the meteorological simulations to investigate future variations in extreme waves induced by TCs around Fiji.

Methods/Experimental

Data

This study uses the National Centers for Environmental Prediction (NCEP) FNL (Final) Operational Global Analysis (NCEP FNL) for the initial and boundary conditions of the hindcast weather simulation of TC Tomas and the base state of the PGW conditions. NCEP FNL provides data with a spatial resolution of 1° × 1° at a time interval of 6 h. The FNL product is generated on a six-hourly basis by the global data assimilation system (GDAS) at NCEP from 1999 to a near-current date. Observational data from the Global Telecommunications System (GTS) and other sources are used in GDAS. The FNL is made with the same model used in the Global Forecast System (GFS), although it is prepared approximately 1 h after the GFS is initialized. Thus, more observational data are accounted for in the analysis. The analyses are available at the surface, 31 pressure levels from 1000 millibars to 1 millibar, and other specific layers as the tropopause, cloud bottom level, cloud top level, and several other levels. The parameters include surface pressure, sea level pressure, geopotential height, temperature, sea surface temperature (SST), soil values, ice cover, relative humidity, u- and v-winds, vertical motion, vorticity, and ozone (NCEP 2018).

The present simulation used SSTs from the National Oceanic and Atmospheric Administration (NOAA) Optimum Interpolation 1/4 Degree Daily SST (NOAA OI SST) analysis data (Reynolds et al. 2007) as a lower boundary condition for the numerical weather simulations. The NOAA OI SST is a dataset that combines different types of observation (satellites, ships, and buoys). In situ data from ships and buoys are used for the large-scale adjustment of satellite biases. The product uses SSTs from the advanced very high resolution radiometer (AVHRR) and Advanced Microwave Scanning Radiometer on the Earth Observing System (AMSR-E). The spatial resolution of the product is 0.25° × 0.25°, which is higher than that of the NCEP FNL reanalysis product.

The PGW conditions consist of the NCEP FNL data and future climate projections from five different GCMs that were developed for CMIP5 (Taylor et al. 2012). In CMIP5, several scenarios of atmospheric greenhouse gas concentrations (i.e., representative concentration pathways; RCPs) were applied to generate future projections under different climate conditions. In this study, future projections based on the RCP8.5 scenario were used for preparation of the PGW conditions. In the RCP8.5 scenario, the radiative forcing of the Earth in the year 2100 is 8.5 W/m^2 greater than the preindustrial level. Based on the evaluation of climate models in CMIP5 report (Flato et al. 2013), reproducibility of SST was investigated for 20 available GCM projections, and five GCMs, which exhibited the better reproducibility of SST than the others, were selected to prepare PGW conditions. The five GCMs used in this study are listed in Table 1.

Numerical weather simulation

The weather research and forecasting (WRF) model version 3.5.1 (Skamarock et al. 2008) was used for the numerical weather simulations. As shown in Fig. 1, two-way, two-level nesting was adopted in this study. The spatial resolutions of the simulations were 30 km and 6 km for the parent (D01) and child (D02) domains, respectively. The number of vertical layers was set to 35 in both domains. The atmospheric pressure at the top boundary of the domain was set to 20 hPa. Various parameterizations are available for each physical process. The parameterization settings in this study are shown in Table 2.

In this study, extreme weather events in a specific area (e.g., around the main island of Fiji, Viti Levu) were investigated by applying the ensemble simulation technique (LSP method described later) to obtain several simulation results. To compare the variations in the characteristics of typhoons and ocean waves in a specific region under different climate conditions, the results of the ensemble simulations must have similar meteorological spatial distributions. Therefore, for D01, a spectral nudging method was applied for atmospheric temperature, zonal wind, meridional wind, and geopotential height every 6 h above a height of 6–7 km.

Wave simulations

The third-generation spectral wave model WaveWatch-III (WW3; Tolman 2009) was used for the wave

Table 1 CMIP5 model outputs used in this study. Data resolution information is obtained from the website of the European Network for Earth system Modeling (2019)

	IPCC ID	Institute (country)	Data resolution (Lon × Lat)
1	GFDL-CM3	Geophysical Fluid Dynamics Laboratory (USA)	2.5° × 2°
2	HadGEM2-ES	UK Met Office Hadley Center (UK)	1.875° × 1.25°
3	IPSL-CM5B-LR	Institute Pierre Simon Laplace	3.75° × 1.8947°
4	MIROC5	Center for Climate System Research (the University of Tokyo), National Institute for Environmental Studies, and Frontier Research Center for Global Change (Japan)	1.40625° × 1.4008°
5	MRI-CGCM3	Meteorological Research Institute, Japan Meteorological Agency (Japan)	1.12148° × 1.125°

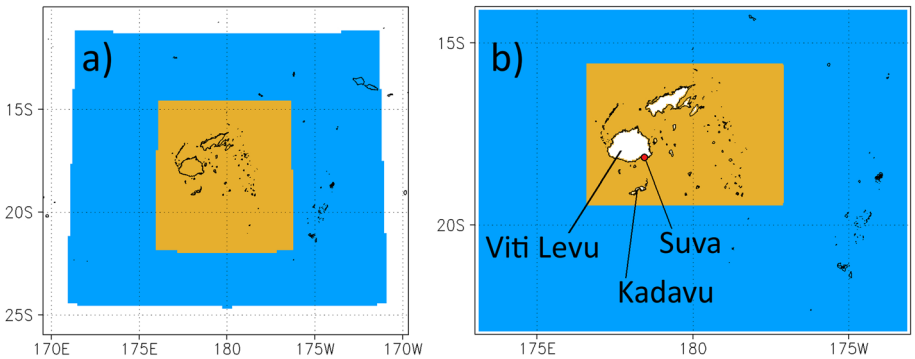

Fig. 1 Domains for the WRF and WW3 simulations. **a** WRF simulations and **b** WW3 simulations. The blue and orange areas represent the parent and child domains, respectively

simulation in this study. A two-domain nesting system was applied to the simulation. The parent domain covered the sea area around the Fiji Islands and their surroundings, while the child domain covered the sea area around the main island (Viti Levu) of Fiji (Fig. 1). The spatial resolutions were 0.1° and 0.033° for the parent and child domains, respectively. In the simulations, the wave spectrum at every computational grid point was discretized to a component of 24 wave directions and 25 wave frequencies from 0.04118 to 0.44617 Hz, with a logarithmic increment of $f(n + 1) = 1.1f(n)$, where $f(n)$ represents the nth frequency. The settings used for WW3 are summarized in Table 3.

Applicability of WW3 for the Central and South Pacific regions was investigated by Durrant et al. (2014). They showed that significant wave height simulated by WW3 agreed well with the buoy observation around Fiji. Their results support confidence of finer resolution WW3 simulation which resolves the required coastal variability.

Table 2 Settings of the WRF simulations

Item	Setting
Version	3.5.1
Horizontal spatial resolution	30 km and 6 km
Cloud microphysics	WRF single-moment 6-class scheme (Hong and Lim 2006)
Cumulus parameterization	Kain-Fritsch scheme (Kain 2004)
Surface layer physics	Revised MM5 surface layer scheme based on the Monin-Obukhov theory with the Carlson-Boland viscous sublayer scheme (Jiménez et al. 2012)
Land surface scheme	Noah land surface model (Chen and Dudhia 2001)
Planetary boundary layer scheme	Bougeault-Lacarrère scheme (Bougeault and Lacarrèr 1989)
Longwave and shortwave radiation	Rapid radiative transfer model (Iacono et al. 2008)

PGW method

Following Sato et al. (2007), the PGW conditions were generated from NCEP FNL and future climatological anomalies using the five GCM projections. As in Sato et al. (2007), future climatological anomalies were calculated as the difference of 10-year monthly mean climate conditions between the future and present. Twenty-year mean climate conditions are often applied in climatological studies; however, 10-year mean conditions were used to include impacts of climate change under advanced global warming conditions. The future 10-year monthly mean climate conditions were calculated from 2091 to 2100 under the RCP8.5 scenario. The present conditions were calculated for 1991–2000 in the historical runs by each GCM. These anomalies were added to the 6-h atmospheric conditions from NCEP FNL. Then, a set of PGW conditions were obtained for wind, atmospheric temperature, geopotential height, and surface pressure. For relative humidity, the original values in NCEP FNL were used in the PGW conditions, and specific humidity under PGW was calculated from the relative humidity and modified atmospheric temperature in

Table 3 Settings of the WW3 simulations

Item	Setting
Grid type	Spherical
Propagation scheme	ULTIMATE QUICKEST propagation scheme with the Tolman averaging technique
Flux computation	Friction velocity according to Ea. 2.35
Linear input	Cavaleri and Malanotte-Rizzoli with filter
Input and dissipation	Tolman and Chalikov (1996) source term package
Nonlinear interaction	Discrete interaction approximation
Bottom friction	JONSWAP bottom friction formulation
Depth-induced breaking	Battjes–Janssen
Bottom scattering	None
Triad interaction	None

the future climate. In the PGW conditions, the ranges and patterns of the temporal variations (e.g., diurnal, seasonal, and interannual variations) of the variables were the same as the reanalysis data and future variations were not included. Even with such a limitation, the PGW method can be easily applied and is useful to investigate the effects and impacts of global warming on the climatological mean conditions. The SSTs for the PGW conditions were generated by adding the SST anomalies obtained from the future and present climates in each GCM to the NOAA OI SST dataset. Using the corresponding number of each GCM in Table 1, the ensemble experiments with the PGW conditions are termed PGW-1, PGW-2, PGW-3, and so on, and the ensemble hindcast is called CTL.

Figures 2 and 3 show composite of atmospheric temperature and geopotential height at 850 and 500 hPa layers for the hindcast and 5 PGW conditions. These atmospheric conditions are parts of initial condition by WRF simulations. There are considerable differences in the atmospheric temperature at 850 and 500 hPa (T850 and T500, respectively) among 5 PGW conditions, but all results show higher T850 and T500 than in the initial condition for the hindcast. In warmer atmospheric condition, saturation specific humidity of atmosphere also increases and more precipitation is expected. Increasing precipitation could cause more latent heat release in TC, and it would sustain TC intensity. Geopotential height at 850 and 500 hPa are also higher in PGW conditions, but atmospheric structure (or horizontal patterns of geopotential height) is similar for the hindcast and PGW conditions.

Figure 4 is spatial distribution of SST at the initial time of the hindcast and 5 PGW simulations. There are significant increases in SST for PGW conditions, and it could provide more heat and moisture flux from the ocean to the atmosphere in PGW conditions. Then, there is high likelihood of intensification of TC. On the other hand, surface heat flux and moisture fluxes are determined by relative difference between the surface and atmosphere, and warmer SST does not always provide large heat and moisture from the ocean.

Ensemble simulation

A new, simple ensemble simulation method (i.e., the LSP method) developed by Taniguchi (2018) was used in this study. The LSP method is based on the lagged average forecasting (LAF) method (Hoffman and Kalnay 1983). The LAF method makes multiple simulations that start at different initial times. In the LSP method, ensemble simulations are conducted in three steps. First, three simulations starting at different initial times are implemented to obtain three base state vectors (X_1, X_2, and X_3) at an appropriate interruption time. Second, two difference vectors (ΔX_2 and ΔX_3) are calculated as the difference between X_2 and X_1 and between X_3 and X_1,

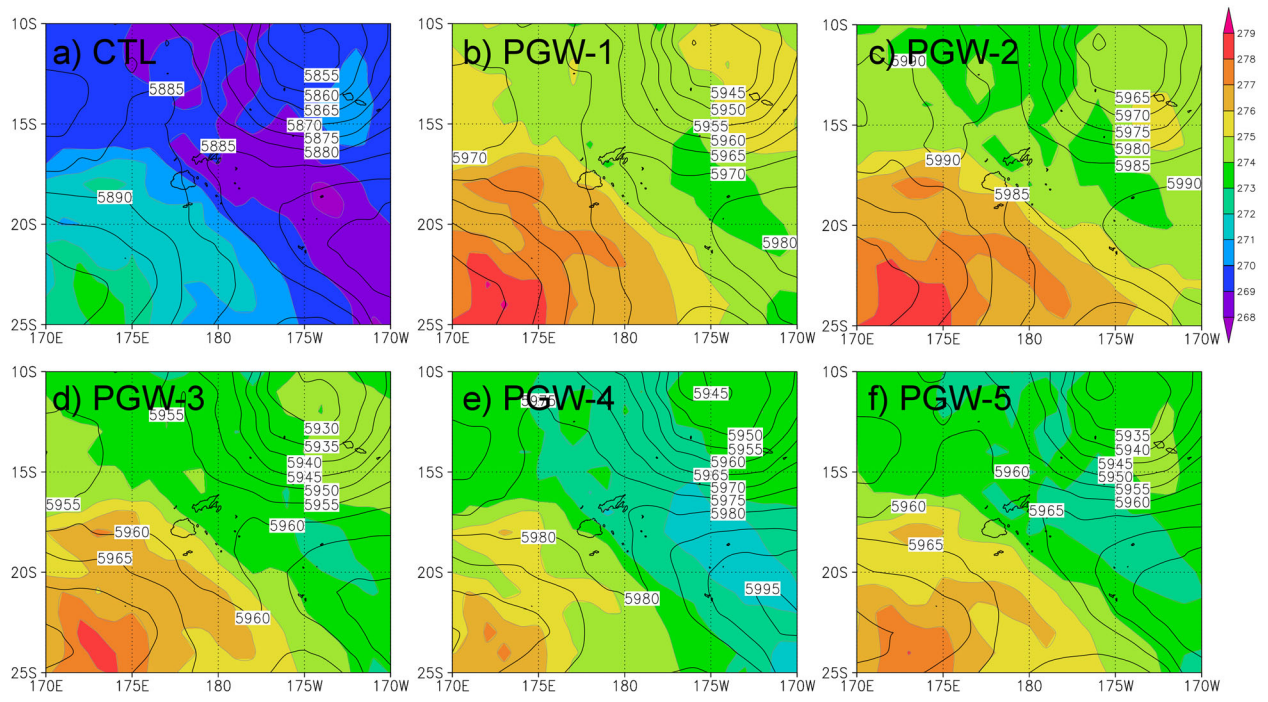

Fig. 2 Spatial distribution of atmospheric temperature and geopotential height at 500 hPa for the initial time. **a** The result of CTL. **b**-**f** The results of each PGW simulation. Shading is atmospheric temperature, and contours are geopotential height. The unit of the color bar is Kelvin

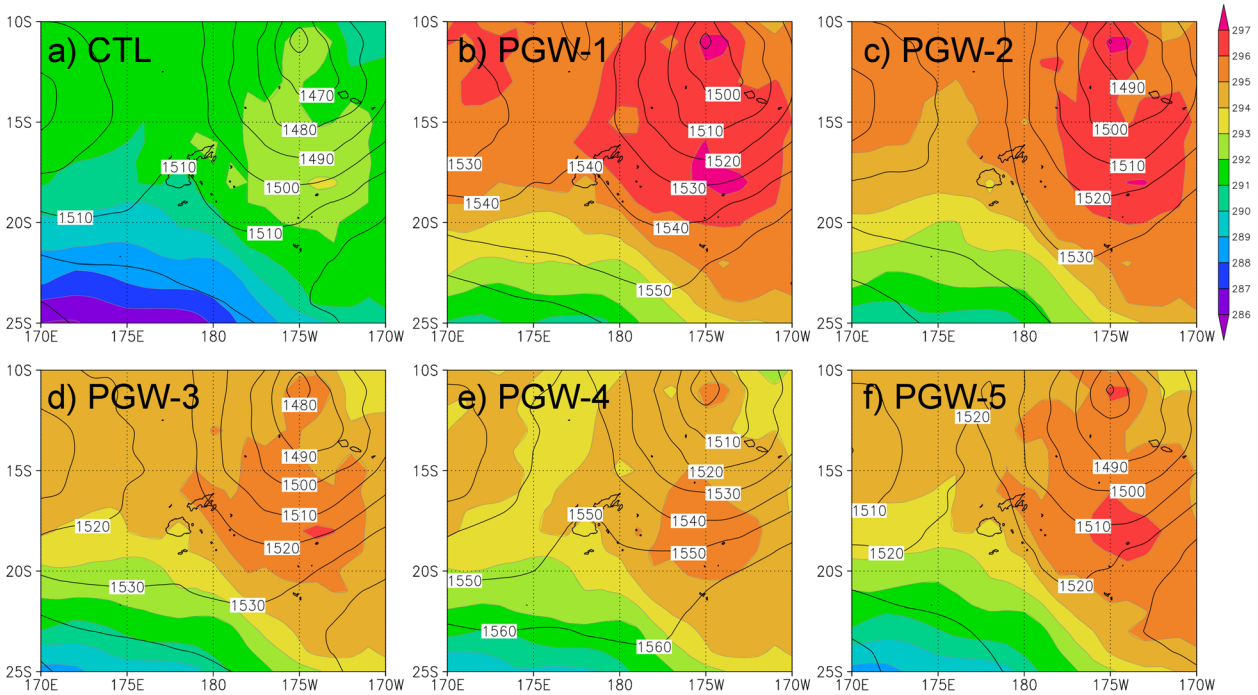

Fig. 3 Spatial distribution of atmospheric temperature and geopotential height at 850 hPa for the initial time. **a** The result of CTL. **b**-**f** The results of each PGW simulation. Shading is atmospheric temperature, and contours are geopotential height. The unit of the color bar is Kelvin

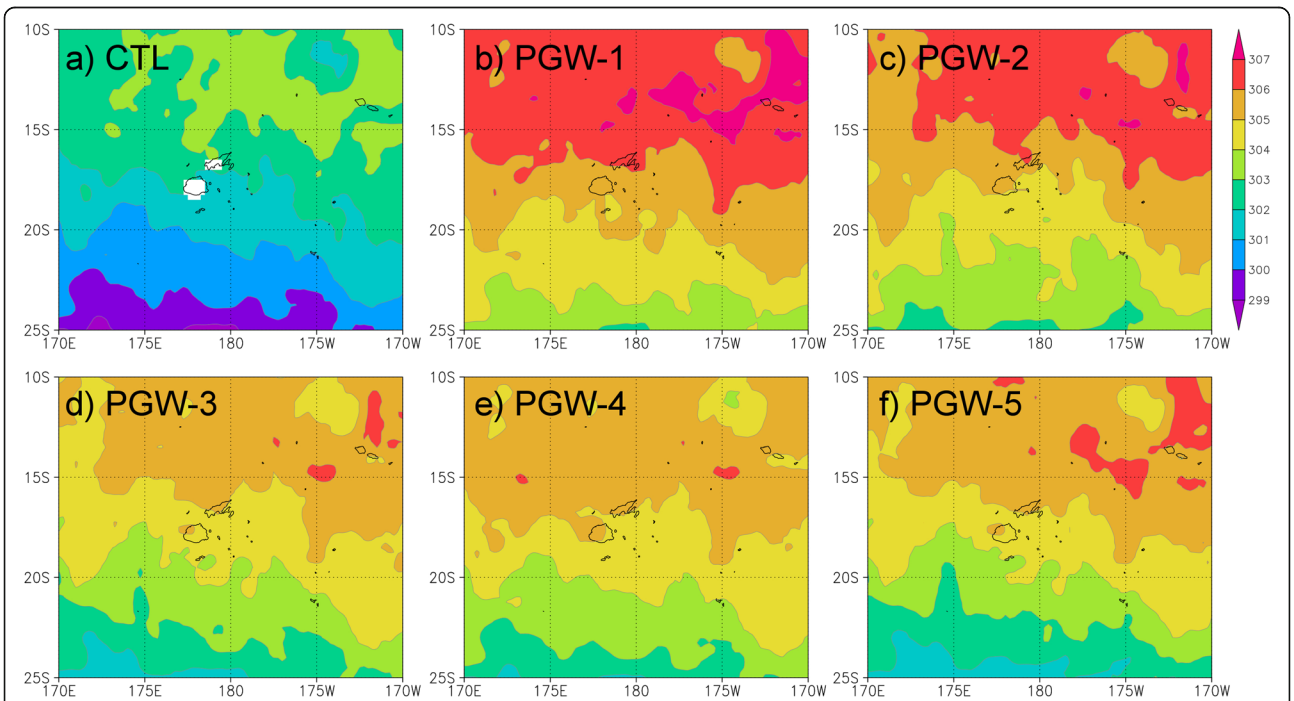

Fig. 4 Spatial distribution of sea surface temperature for the initial time. **a** The result of CTL. **b**-**f** The result of each PGW simulation. The unit of the color bar is Kelvin

respectively. Third, new state vectors (X_n) are prepared from a single base state (X_1) and the two difference vectors (ΔX_2 and ΔX_3) using the following equation:

$$\mathbf{X_n} = \mathbf{X_1} + \alpha\Delta\mathbf{X_2} + \beta\Delta\mathbf{X_3}$$

where α and β represent the scale factors for ΔX_2 and ΔX_3, respectively. Then, the ensemble simulations are conducted from the interruption time with the new state vectors. The initial and interruption times are shown in Table 4. In the new state vectors, atmospheric temperature, zonal and meridional wind components, specific humidity, atmospheric pressure, and SST are updated via the LSP method. The same scale factors (α and β) are applied for all variables. The LSP method is only applied to the initial conditions. The boundary conditions are the same for all ensemble members. The LAF method requires unnecessarily large lags to generate many ensemble members. Furthermore, the LAF method should yield large differences in accuracy depending on the length of the simulations. As shown in Table 4, three simulations have different initial time, but others are started from the same initial time. Therefore, the aforementioned weaknesses of the LAF method are eliminated in the LSP method. The scale factors used in this study are given in Table 5, and 19 members are produced for each ensemble simulation (one present and five future climate simulations).

Table 4 Initial and interruption times of the WRF simulations.

Run	Initial time	Interruption time (generating new ensemble members)	End of simulation
Run to make X_1	00 UTC 11 March	00 UTC 12 March	00 UTC 17 March
Run to make X_2	06 UTC 11 March		
Run to make X_3	12 UTC 11 March		

Table 5 Combination of scale factors (α and β) to produce the ensemble members

Combinations of scale factors (α and β)			
(− 1/3, 1/3)	(− 1/3, 2/3)	(− 1/3, 1)	(0, 1/3)
(0, 2/3)	(1/3, − 1/3)	(1/3, 0)	(1/3, 1/3)
(1/3, 2/3)	(1/3, 1)	(2/3, − 1/3)	(2/3, 0)
(2/3, 1/3)	(2/3, 2/3)	(1, − 1/3)	(1, 1/3)

The three original state vectors (X_1, X_2, and X_3) are excluded

Results and discussion

Hindcast of TC Tomas and ocean waves

Figure 5a shows the track of TC Tomas based on the best track data from the Joint Typhoon Warning Center (JTWC) and the tracks of the hindcast ensemble from WRF. TC Tomas moved from the north to south. In the early stage (i.e., north of 20° S), simulated tracks and the best track agree well with each other. On the other hand, south of 20° S, the simulated tracks are slightly moved from the best track in the eastward direction. However, the track of TC Tomas is reproduced well in the WRF simulations because of the effect of the spectral nudging. Figure 5b shows the temporal variations in the central pressure of TC Tomas. The central pressure of the best track data reaches a minimum central pressure of 937 hPa, whereas the ensemble mean central pressures of the present simulation yields a minimum pressure of 949.8 hPa, and the lowest minimum central pressure of the 19 ensemble members is 932.9 hPa. These results indicate that several ensemble members duplicate strong TCs that are as intense as actual TC Tomas (or the JTWC result). Although the time profile of the simulated central pressure appears to be delayed for approximately 1 day compared with that of the best track data, the simulated profile reasonably captures the decreasing slope and minimum central pressure of the best track data. Several studies have shown delayed intensification of simulated TCs (Oku et al. 2010; Takayabu et al. 2015; Nasuno et al. 2016; Kanada et al. 2017b; Nayak and Takemi 2019). Takayabu et al. (2015) indicated the effect of initial and boundary conditions on TC simulations. Nayak and Takemi (2019) also highlighted the role of initial and boundary conditions in delayed TC development. Moreover, Nasuno et al. (2016) showed that small latent heating differences over the ocean can delay the development of TCs. Kanada et al. (2017b) indicated that sea surface cooling can suppress the delayed evolution of the simulated TCs. However, it is not the main scope of this study to improve the boundary condition (SSTs) and surface physics schemes. Therefore, the future simulations were conducted based on the results shown in Fig. 5.

Figure 6 shows the spatial distribution of the simulated and observed surface wind speeds around Fiji. The observed wind speed was obtained from Advanced Microwave Scanning Radiometer for EOS (AMSR-E) onboard the Earth observation satellite Aqua (Shibata 2006). To compare the overall structure of TC Tomas, the WRF simulation results are extracted from the parent domain. At 14 UTC on 15 March 2010, the peaks of the sea surface wind speeds based on the AMSR-E and WRF simulations are located in nearly the same place, and the peak wind speeds obtained from the AMSR-E and WRF simulations are comparable, although the area of relatively strong wind is wider in the WRF simulation than in the AMSR-E-based observations. At 02 UTC on 16 March, the WRF simulation result shows a larger wind speed near the center of TC Tomas and a wider area of relatively high wind speed compared to the AMSR-E-

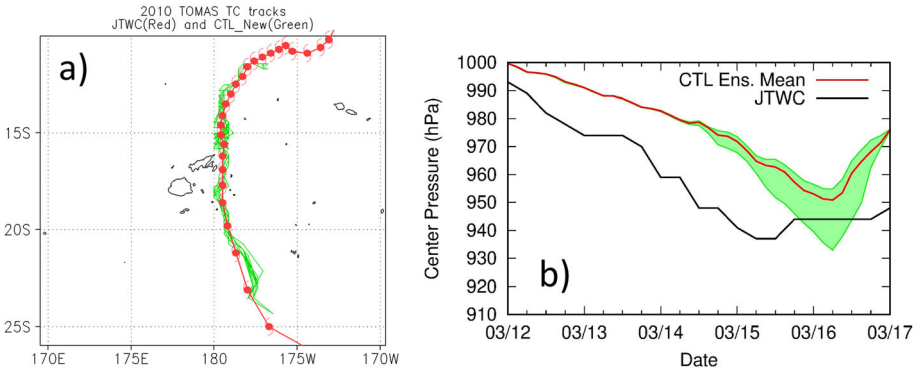

Fig. 5 Tracks and center pressures of TC Tomas. **a** Tracks of TC Tomas. The red line represents the best track by JTWC. The green lines represent the results of the ensemble simulation. **b** Temporal variations in the center pressure of TC Tomas. The black line represents the result of the best track by JTWC. The red line indicates the ensemble mean center pressure. The range of the ensemble spread is represented by green shading

based observation. The maximum wind speed in the 19 ensemble CTL simulations is 53.1 to 65.3 m/s. In the best track, the maximum wind speed is 59.2 m/s for TC Tomas, which is comparable to the result of the CTL ensemble simulation.

Figures 5 and 6 show good agreement in the central pressure and surface wind speed, respectively, between the WRF simulation and the observations at 02 UTC on 16 March, but there are some differences at 14 UTC on 15 March. Although there are some differences between the observed and simulated results of TC Tomas, the present WRF simulations reasonably capture the characteristics of TC Tomas. Thus, this study uses the present WRF simulation to investigate variations in the wind field under warmer climate conditions.

Using the WRF simulation results to force the model, wave simulations are implemented by WW3. Figure 7 shows the spatial distribution of the ensemble mean maximum wind speed in CTL. A strong wind greater than 45 m/s is recognized southeast of the main island

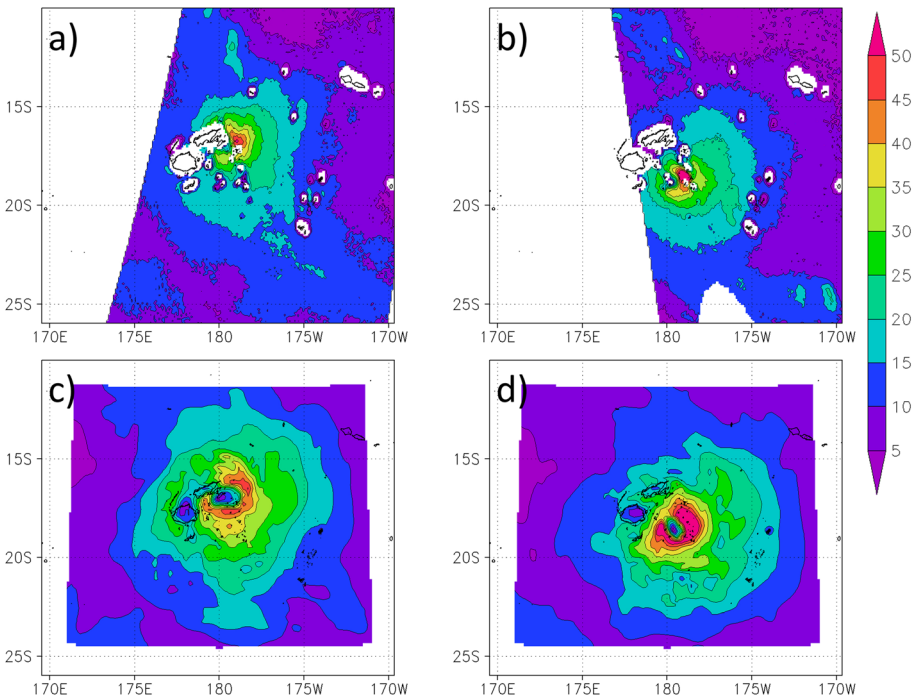

Fig. 6 Comparison of the wind speed around the Fiji Islands. **a** AMSR-E sea surface wind at 14 UTC on 15 March, **b** AMSR-E sea surface wind at 02 UTC on 16 March, **c** WRF 10 m wind speed at 14 UTC on 15 March, and **d** WRF 10 m wind speed at 02 UTC on 16 March. The unit of the color bar is m/s

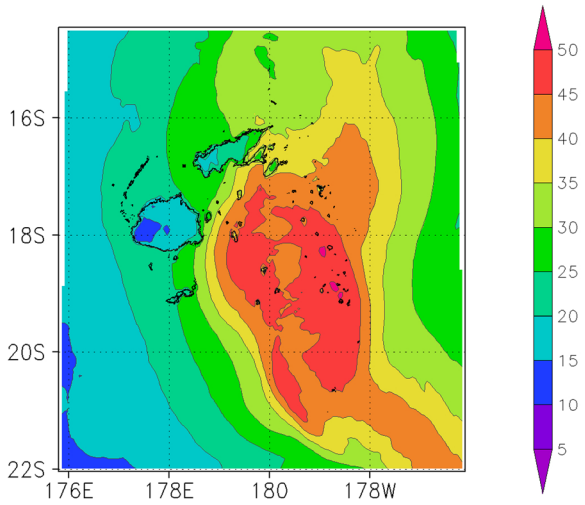

Fig. 7 Spatial distribution of the ensemble mean maximum wind speed in the CTL. The unit of the color bar is m/s

of Fiji (Viti Levu). The spatial distribution of the ensemble mean maximum significant wave height (H_s) in CTL shows significantly high waves in the area of strong wind (Fig. 8a). The maximum H_s in the target domain is from 15.2 to 18.9 m southeast of Viti Levu. Figure 8b shows the temporal variation in H_s around the offshore region of Suva (178.47° E, 18.20° S). The maximum H_s around Suva ($H_{s\_\max}$) appears at approximately 00 UTC on 16 March. The ensemble mean $H_{s\_\max}$ is 8.63 m, and the maximum $H_{s\_\max}$ in the 19 ensemble members is 9.26 m. In the case of TC Tomas, there is no observation data for ocean waves. In Barstow and Haug (1994), the observation value of the ocean waves induced by TCs around Fiji is recorded. In December 1992, TC Joni passed through the western region of Fiji, and the maximum 1 (10) minute mean wind speeds were 56.9 (45.8) m/s. In the case of TC Joni, the maximum Hs southwest of Kadavu Island (located south of Viti Levu, see Fig. 1b) was 7.2 m. In the case of TC Tomas, the maximum 1-min and 10-min means of the wind speed were 59.2 m/s and 51.4 m/s, respectively. The stronger wind from TC Tomas could cause a larger H_s than that from TC Joni, which is consistent with the present results based on the WW3 computations.

Variations in TC Tomas and ocean waves in the future

Figure 9 compares the TC tracks of CTL and the five PGW ensemble simulations. The tracks of PGW-2, PGW-3, PGW-4, and PGW-5 match well with the best track. While the simulated TC track of PGW-1 slightly shifts eastward south of 17.5° S, the simulated TC track agrees reasonably well with the best track data. All five PGW ensemble simulations give tracks that are approximately similar to that of TC Tomas in CTL.

The temporal variations in central pressure of the simulated TC are shown in Fig. 10. In PGW-1 and PGW-5, the ensemble mean minimum central pressure ($\overline{P}_{\min}$) is lower than that in the CTL. The minimum values of central pressure among the 19 ensemble members in PGW-1 and PGW-5 are also lower than those in CTL. These results indicate the apparent intensification of the TC in PGW-1 and PGW-5. The ensemble mean minimum central pressure is slightly lower in PGW-2 and PGW-4 than that in CTL, and the minimum values are no smaller than those in CTL. The minimum value of the ensemble mean time series in PGW-3 is nearly equal to that of the CTL. The ensemble spread, indicated by shading in Fig. 10, shows that the most intense ensemble member in PGW-3 is also comparable to CTL. Difference of T500 and T850 (or T500-T850) averaged over the region of 178E-178W, 14S-22S is shown in Table 6. In PGW-2 and 3, the difference of the two layers is smaller than the other simulations. Difference of T850 and SST (or T850-SST) for the same region is also smaller in PGW-2 and 3 (Table 6). These results

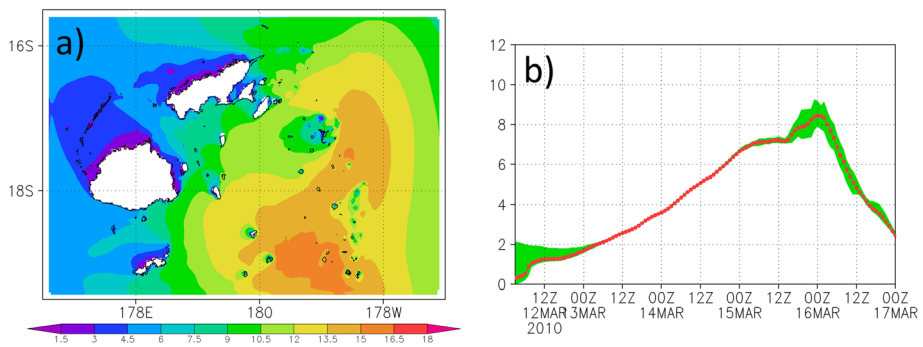

Fig. 8 WW3 simulation results. **a** Spatial distribution of the ensemble mean maximum significant wave height in the CTL. The unit of the color bar is m. **b** Temporal variation in the significant wave height over the offshore region of Suva in the CTL. The red line represents the ensemble mean value. Green shading indicates the range of the ensemble spread. The unit for the vertical axis is m

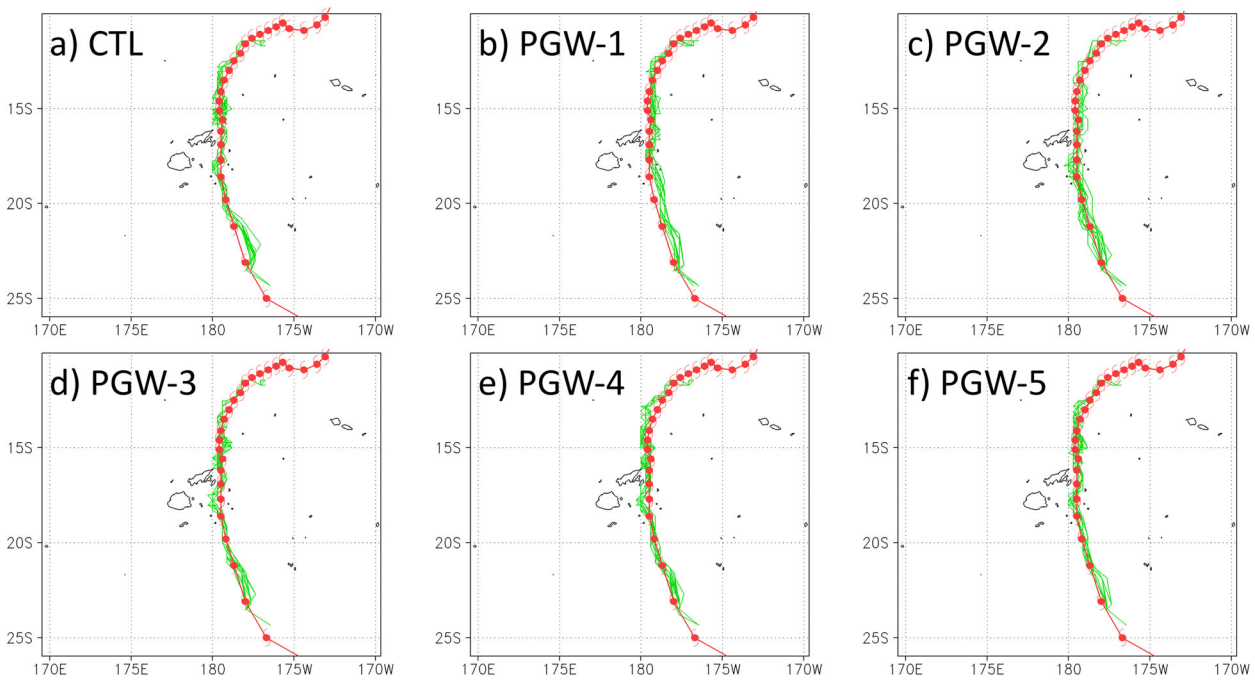

Fig. 9 Tracks of TC Tomas in the CTL and five PGW ensemble simulations. **a** The result of CTL. **b**-**f** The results of each PGW simulation. The red line represents the best track by JTWC. The green lines represent the results of the ensemble simulation

indicate more stable atmospheric stratification and smaller upward heat flux in PGW-2 and PGW-3. As shown in Figs. 2 and 3, atmospheric temperature and SST are higher in all PGW conditions, and intensification of TC is expected in PGW simulations. But more stable and smaller heat flux could prevent TC intensification.

Figure 11 shows the difference in the ensemble mean maximum wind speed between CTL and the five PGW ensemble simulations. While the TC was intensified in

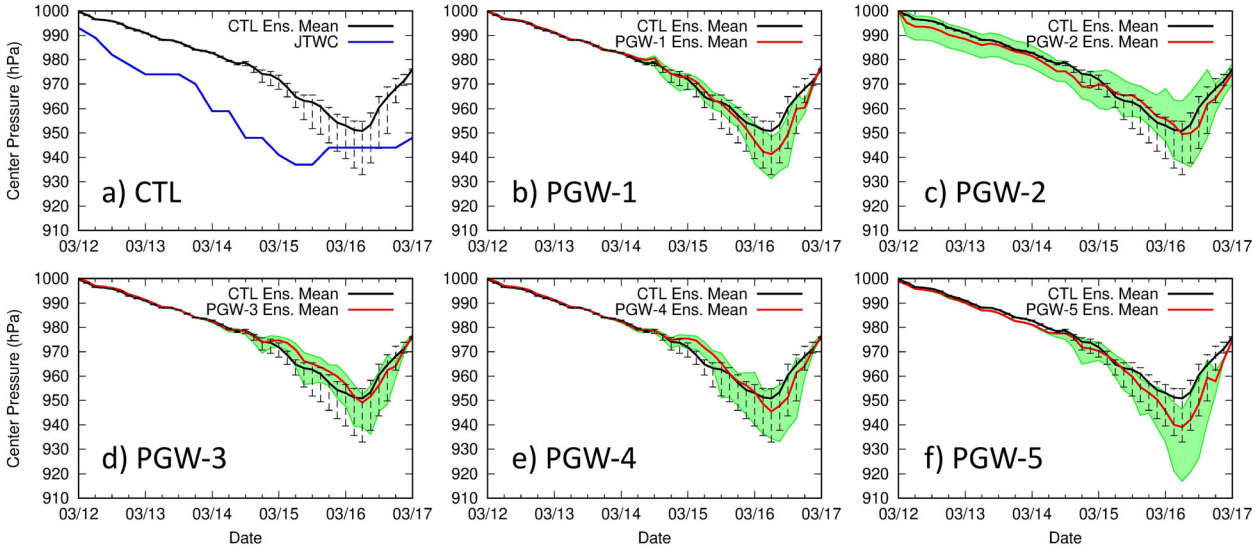

Fig. 10 Temporal variations in the center pressure of TC Tomas in the CTL and PGW simulations. **a** The black line is ensemble mean center pressure of the CTL. Dashed vertical bars indicate the ensemble spread of the CTL. The blue line is center pressure of JTWC. **b**–**f** The results of each PGW simulation. The red line and the green shading indicate the ensemble mean center pressure and the range of the ensemble spread, respectively. The result of the CTL is also shown in each panel

Table 6 Difference of atmospheric temperature at 500 hPa and 850 hPa (T500-T850), and difference of atmospheric temperature at 850 hPa and sea surface temperature (T850-SST)

	CTL	PGW-1	PGW-2	PGW-3	PGW-4	PGW-5
T500-T850	− 21.4	− 20.3	− 19.8	− 19.9	− 21.0	− 20.3
T850-SST	− 32.2	− 30.4	− 29.9	− 29.9	− 31.5	− 30.6

Results are average for 178E-178W, 14S-22S

PGW-1 (Fig. 10), the ensemble mean wind speed in PGW-1 is smaller than that in CTL southeast of Viti Levu (Fig. 11b). This feature may be caused by an eastward shift in the TC track in PGW-1 (Fig. 11b). In another intensified TC simulation (PGW-5), the wind speed becomes larger in the wider area of domain 2. PGW-2 and PGW-4 show similar variations in the central pressure, but the spatial distributions of the wind speed are quite different. In PGW-4, significant increases in the maximum wind speed are recognized, and a weakened wind is found in limited areas. On the other hand, the ensemble mean maximum wind speed becomes weaker than that in the CTL in a wide area in PGW-2. The minimum peak in the central pressure in PGW-2 occurs later than that in CTL (Fig. 10c), and an increased wind speed is found near the southern boundary of domain 2. These results indicate that the development of the TC delays PGW-2 and that the wind speed is weaker around Fiji. The other four PGW simulations show almost the same timing of the minimum peak in the ensemble mean central pressure as CTL. In PGW-3, an enhanced wind is found around Viti Levu, and a weakened wind occurs east of these areas, which can be caused by a slight westward shift in the track in PGW-3 (Fig. 11d).

Variations in the ensemble mean maximum H_s ($\overline{H}_{s\_\max}$) in the PGW simulations are shown in Fig. 12. Generally, increasing and decreasing $\overline{H}_{s\_\max}$ correspond to variations in wind speed, as shown in Fig. 11. In PGW-3, PGW-4, and PGW-5, significant increase in $\overline{H}_{s\_\max}$ (larger than 0.8 m) is found over the southeastern coast of Viti Levu. In PGW-1, the eastward shift in the TC track results in a significant increase in $\overline{H}_{s\_\max}$ over the southeast edge of domain 2 and a decrease southeast of Viti Levu. In PGW-2 because of the decreased wind speed shown in Fig. 11, $\overline{H}_{s\_\max}$ is smaller than that in CTL. As discussed in the previous subsection, such a decreasing $\overline{H}_{s\_\max}$ in domain 2 may be because of the slower development of the TC in PGW-2.

Figure 13 shows the temporal variation in H_s around the offshore region of Suva (178.47° E, 18.20° S) in the CTL and five PGW simulations. The ensemble mean Hs

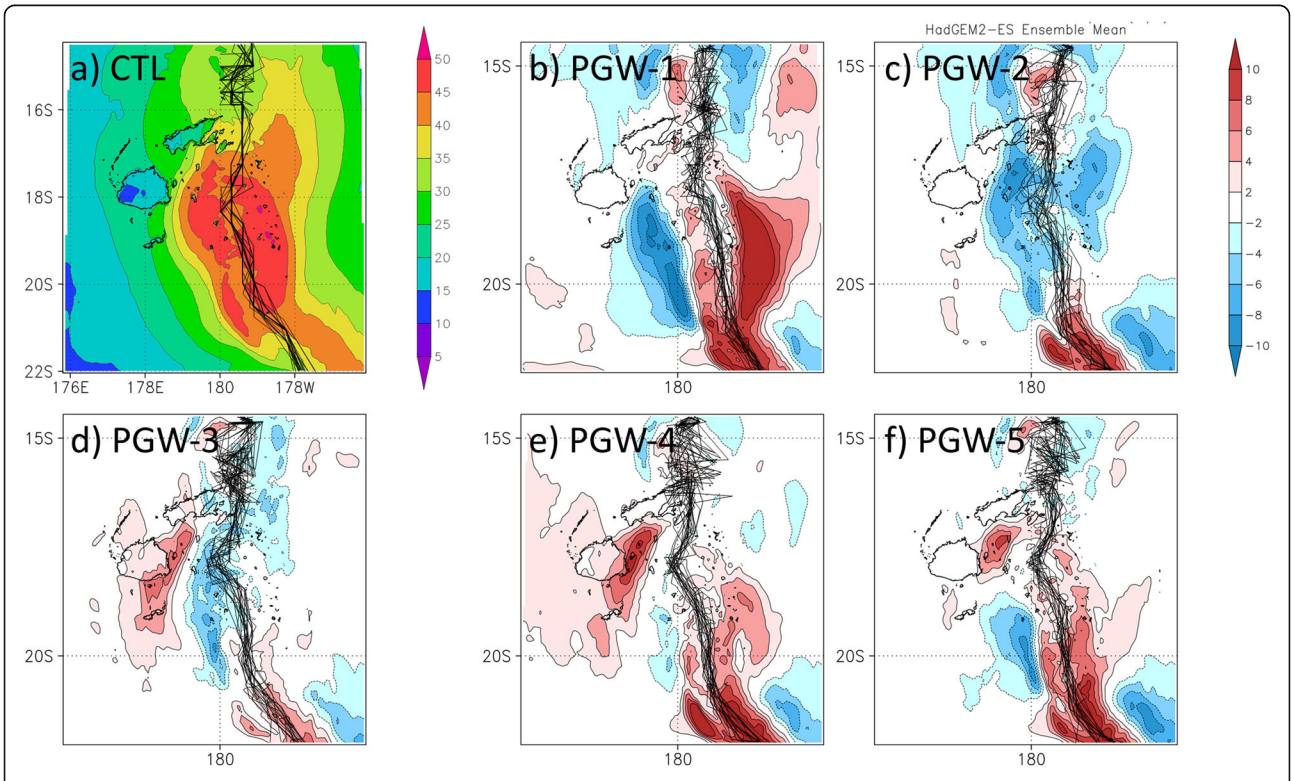

Fig. 11 Spatial distribution of the ensemble mean maximum wind speed. **a** CTL results (same as Fig. 4). **b**–**f** Difference in the ensemble mean maximum wind speed between the CTL and each PGW ensemble simulation. The unit of color bar is m/s

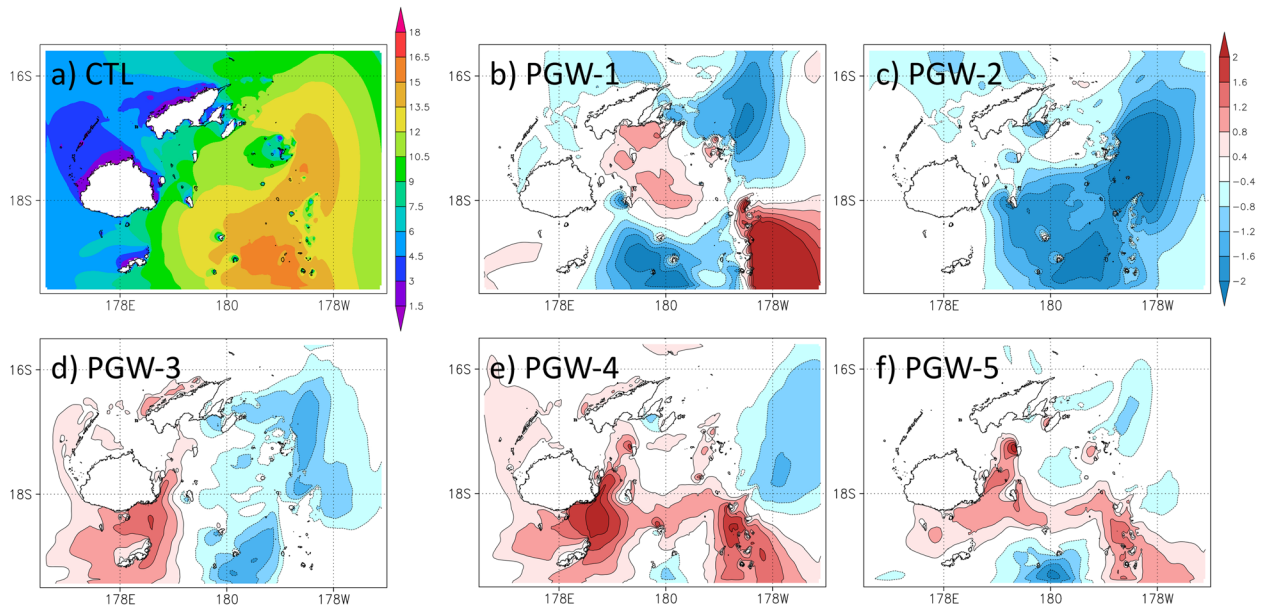

Fig. 12 Spatial distribution of the ensemble mean maximum significant wave height. **a** CTL results (same as Fig. 5a). **b**–**f** Difference in the ensemble mean maximum significant wave height between the CTL and each PGW ensemble simulation. The unit of the color bar is m.

in PGW-1 shows faster enhancement than that in CTL, but the maximum value in PGW-1 is the same as that in CTL. At the same time, the ensemble spread (indicated by shading) is also the same as that of the CTL. In PGW-2, the peak of the ensemble mean H_s is the same as that of the CTL. However, the maximum peak in H_s in the PGW-2 ensemble is more than 1 m larger than that in the CTL. In PGW-3, PGW-4, and PGW-5, the peak of the ensemble mean H_s is clearly larger than that in the CTL. Even in the minimum case, the peak of H_s is larger than that in the CTL in these three PGW simulations.

Figure 14 shows histograms and the probability density curves of the maximum significant wave height (H_{s_max}) around Suva in the CTL and five PGW simulations. Here, the probability densities were calculated based on the assumption of a normal distribution. The CTL results show a peak at approximately 8.5 m, and the range

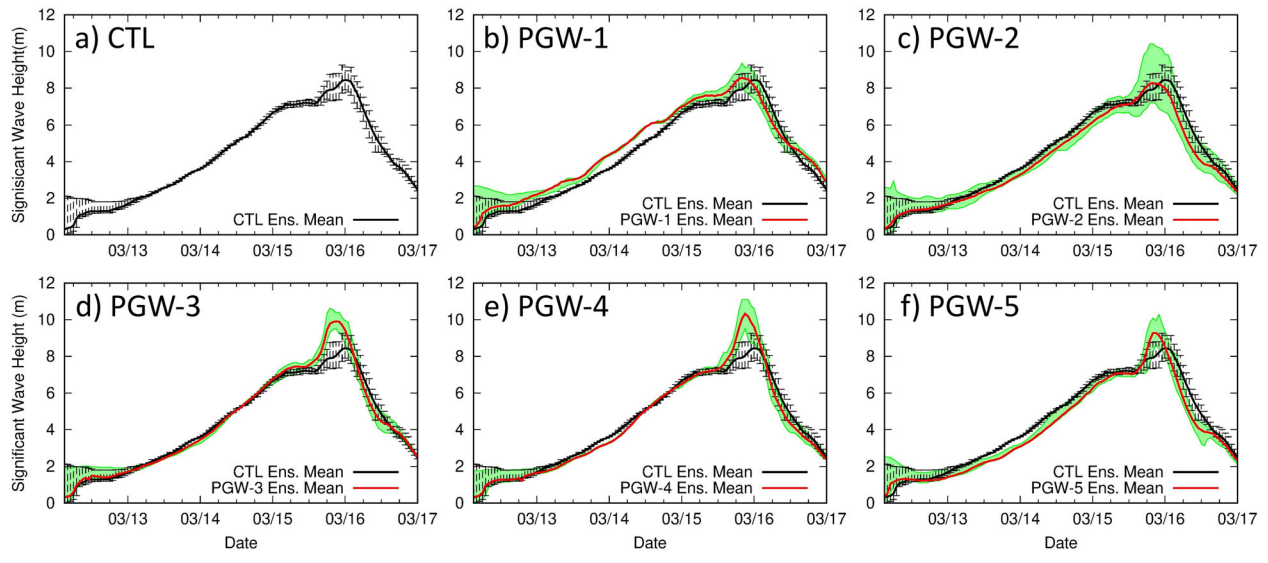

Fig. 13 Temporal variation in the significant wave height over the offshore region of Suva. **a** The result of CTL. Black line and dashed vertical bars indicate the ensemble mean value and the ensemble spread, respectively. **b**–**f** The results of each PGW simulation. The red line and the green shading represent the ensemble mean value and the range of the ensemble spread, respectively. The result of the CTL is also shown in each panel

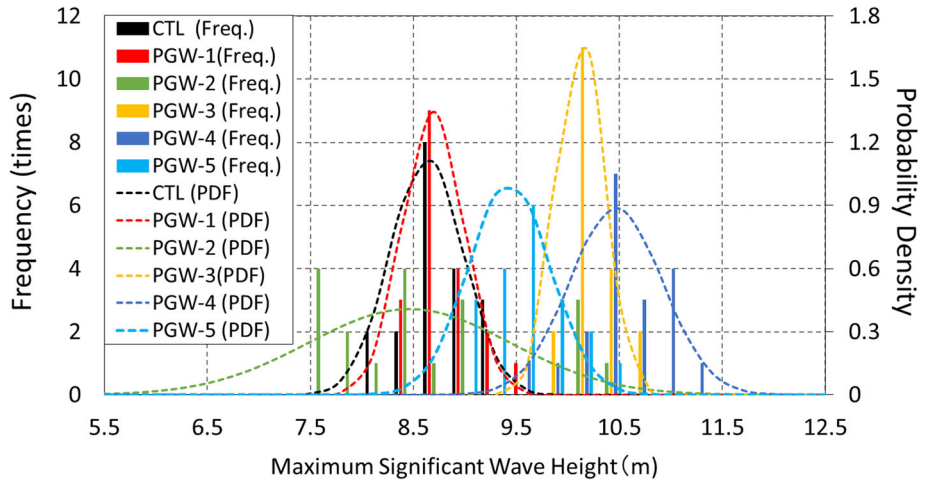

Fig. 14 Histograms ("Freq.") and probability density function (PDF) curves of the maximum significant wave height. Results are for the offshore region of Suva in the CTL and five PGW simulations

of $H_{s\_\max}$ is from 7.5 to 9.5 m. PGW-1 shows similar results to the CTL. In PGW-2, the probability density peak of $H_{s\_\max}$ is the same as that in the CTL, but the $H_{s\_\max}$ spread is much wider than that in other ensemble simulations. This result indicates that in some global warming conditions, the average of the extremes is the same as the present climate, but a significantly severe case can occur under particular conditions. In PGW-3, PGW-4, and PGW-5, frequency peaks are found at a significantly larger $H_{s\_\max}$ than those in the CTL. The results of these three PGW ensemble simulations indicate that, when a TC similar to Tomas occurs in a future climate, it will make much larger ocean waves, which could cause severe disasters. Especially in PGW-3 and PGW-4, the histogram and probability density curves hardly overlap with those of the CTL, and $H_{s\_\max}$ around Suva reaches an unexpected scale in the present climate with high probability.

A summary of the CTL and PGW ensemble simulations is shown in Table 7. PGW-4 and PGW-5 indicate an intensified TC and larger H_s near the offshore region of Suva in a future climate. The results of PGW-1 and PGW-2 also show a somewhat enhanced TC, but H_s near the offshore region of Suva is comparable to that of the CTL. On the other hand, the intensity of the TC in PGW-3 is similar to that in the CTL, but H_s is quite larger than that in the CTL. Significantly high ocean waves and larger storm surges are expected in PGW-4 and PGW-5. PGW-1 and PGW-2 show a high possibility of a larger storm surge, but ocean waves are as high as those in the present climate. In PGW-3, the scale of the storm surge is expected to be the same as that in the CTL, but higher ocean waves are expected in the future climate.

In Table 7, standard deviations and medians are also shown for the minimum central pressure ($P_{\min}$), maximum wind speed ($U_{\max}$), and maximum H_s in the offshore region of Suva ($H_{s\_\max}$). In many PGW simulations, the standard deviations are smaller than those in the CTL for $P_{\min}$, $U_{\max}$, and $H_{s\_\max}$. Some PGW simulations show larger standard deviations, but they are comparable to those of the CTL. At the same time, the medians for these three variables are almost the same as the ensemble mean values. Thus, the future intensification of TCs and higher ocean waves are not caused by rare extreme events, but they exist with high probability when they do occur.

Table 7 Summary of the WRF and WW3 simulations

		CTL	PGW-1	PGW-2	PGW-3	PGW-4	PGW5
$P_{\min}$ (hPa)	Average	949	**938**	**942**	**947**	**942**	**936**
	Min	932	931	936	936	921	917
	Max	953	946	952	951	950	945
	Std. Dev.	5.0	3.8	4.7	3.7	6.3	6.0
	Median	950	938	941	948	942	937
$U_{\max}$ (m/s)	Average	56	**63**	**58**	**57**	**62**	**62**
	Min	51	60	55	54	57	57
	Max	65	67	61	61	67	71
	Std. Dev.	2.9	2.0	1.7	2.0	2.9	3.2
	Median	55	63	58	57	62	61
$H_{s\_\max}$ (m)	Average	8.6	**8.7**	8.5	**10.1**	**10.5**	**9.4**
	Min	7.9	8.2	7.3	9.8	9.5	8.8
	Max	9.3	9.3	10.4	10.6	11.1	10.3
	Std. Dev.	0.35	0.30	0.98	0.23	0.45	0.40
	Median	8.6	8.6	8.2	10.0	10.4	9.4

All values are calculated from 19 ensemble members of the CTL and five PGW simulations. Average values larger than the result of CTL are shown in bold font

The results in Table 7 indicate various types of hazards under global warming. For sufficient risk assessment near coastal areas, various mixed hazards and their possibilities have to be evaluated based on ensemble simulations using multiple GCM outputs.

Conclusions

Based on TC Tomas in 2010, ensemble PGW simulations were implemented to investigate future variations in the characteristics of TCs and induced ocean waves around Fiji. Five GCM projections were used to produce PGW conditions for future simulations. The ensemble mean minimum central pressures of TCs in four PGW simulations are smaller than those in the hindcast (CTL). In three of the five future simulations, the tracks and development of the TC are similar to those of the CTL. In these PGW simulations, a significant increase in the maximum significant wave height was recognized southeast of the Fiji main island (Viti Levu). In the case of an eastward shift in the track in PGW-1, the significant wave height was smaller than that of the CTL around Viti Levu, but higher in the more eastern regions. In PGW-2, the delayed development of the TC caused a lower significant wave height around Fiji but a higher wave height in the southern region. In PGW simulations whose maximum significant wave height is larger than the hindcast (or PGW-3, 4, and 5), the probability density of the maximum significant wave height in the offshore region of Suva (i.e., the southern part of Viti Levu) showed that when a TC similar to Tomas occurs in future climate, there will be significantly larger ocean waves, which are not expected under the present climate. Two PGW simulations showed very different probability density curves from those of the CTL, which indicates the high probability of a significant wave height dominating the maximum in the present climate. At the same time, in PGW-2, where the ensemble mean maximum wave heights are similar to those in the CTL, a wider variability was found. This result indicates that variability of ocean waves would be larger and extremely high ocean waves would be more likely to occur under the condition of global warming. In this study, future variation of TC frequency is not considered. For assessment of effects of future variations in TC and ocean waves, it is necessary to combine frequency of TC occurrence and changes in characteristics of extreme events.

Five PGW simulations showed different types of characteristics of TCs and ocean waves in a future climate: large ocean waves and lower surface pressure (which cause large storm surge), large ocean waves with moderate pressure, and moderate ocean waves with lower surface pressure. These results indicate the importance of using future projections from multiple GCMs to make an adequate evaluation of risk assessments and possible hazards. For a more comprehensive assessment, more GCM projections and other global warming scenarios should be applied for various TC events. By focusing on a specific area or place, a small difference in the TC track might significantly affect the results of the wave simulations or the evaluation of hazards induced by TCs. Shimura et al. (2015) suggested the importance of TC track shifts. In addition to various patterns of TC characteristics using multiple GCM projections, considering a number of TC tracks is crucial for risk assessment. At the same time, there are limitations in numerical weather simulations. First, as stated in the methodology, same lateral boundary conditions were applied for all ensemble members based on the LSP method. Second, the spectral nudging was applied to obtain similar TC tracks among the hindcast and PGW simulations. These limitations may make ensemble spread smaller and reduce the degree of freedom in TC simulations. To increase the number of TC samples and reduce the effect of these limitations, application of stochastic technique may be useful. In this study, possible future variations of TC characteristics and induced ocean waves were investigated through the case study of TC Tomas. For more comprehensive understanding of impacts of global warming on extreme TCs and ocean waves, it is indispensable to increase the number of similar numerical simulations of various TC events. In WRF simulations, physical processes in the ocean and upwelling water along TC are not fully resolved. It may cause overestimation of SST and intensity of TCs. Simulations by atmosphere-ocean coupled model is also important to consider more detailed processes of TC development and to enhance the accuracy in estimation of global warming impacts. At the same time, a technique to translate the results from numerous ensemble simulations and probability information has to be established for designing measures for mitigation and adaptation.

Abbreviations

AMSR-E: Advanced Microwave Scanning Radiometer on the Earth Observing System; AVHRR: Advanced very high resolution radiometer; CMIP5: Couples Model Intercomparison Project Phase 5; GCM: Global climate model; GDAS: Global data assimilation system; GFS: Global Forecast System; GTS: Global Telecommunication System; JTWC: Joint Typhoon Warning Center; LSP: Lagged-simulated perturbation; NCEP FNL: NCEP Final Operational Global Analysis; NCEP: National Centers for Environmental Prediction; NOAA: National Oceanic and Atmospheric Administration; PGW: Pseudo global warming; RCP: Representative concentration pathways; SST: Sea surface temperature; TC: Tropical cyclone; WAM: (a third generation) Wave model; WRF: Weather research and forecasting; WW3: WaveWatchIII

Acknowledgments

The authors are grateful to all of the data providers. The NCEP FNL Operational Global Analysis data are available at the Research Data Archive at the University Corporation for Atmospheric Research (UCAR). The NOAA OI SST products obtained from NCEP at NOAA. The CMIP5 products are distributed from several CMIP5 data portals. We are also appreciative of the

AMSR-E wind and JTWC products. This research was based on an activity supported through the Ministry of Environment in Japan.

Authors' contributions

KT conceived and designed the study, implemented the numerical simulations, and analyzed the simulation results. YT proposed the topic and collaborated with the corresponding author in the construction of the manuscript. Both authors read and approved the final manuscript.

Funding

This research was based on an activity to develop a methodology for the evaluation of climate change impacts on storm surge and storm wave hazards supported through the Ministry of the Environment in Japan.

Availability of data and materials

The datasets used as initial and boundary conditions for the WRF simulations are available in the repository of each product (NCEP FNL: https://rda.ucar.edu/datasets/ds083.2/, NOAA OI SST: https://www.ncdc.noaa.gov/oisst, CMIP5: https://esgf-node.llnl.gov/projects/cmip5/). The best track data of tropical cyclones are distributed by the Joint Typhoon Warning Center through the Naval Oceanography Portal (https://www.metoc.navy.mil/jtwc/jtwc.html). Please contact the author for the AMSR-E sea surface wind product.

Competing interests

The authors declare that they have no competing interest.

Author details

[1]Faculty of Geosciences and Civil Engineering, Kanazawa University, Kakuma-machi, Kanazawa, Ishikawa 920-1192, Japan. [2]Department of Civil Engineering, The University of Tokyo, 7-3-1 Hongo, Bunkyo, Tokyo 113-8656, Japan.

Received: 2 August 2019 Accepted: 22 January 2020
Published online: 18 February 2020

References

Appendini CM, Pedrozo-Acuña A, Meza-Padilla R, Torres-Freyermuth A, Cerezo-Mota R, López-González J, Rioz-Salcines P (2017) On the role of climate change on wind waves generated by tropical cyclones in the Gulf of Mexico. Coastal Eng J 59:174001. https://doi.org/10.1142/S0578563417400010

Barstow SF, Haug O (1994) Wave in climate in Fiji, SOPAC Technical Report, 205. Oceanographic Company of Norway, Trondheim

Bell SS, Chand SS, Tory KJ, Dowdy AJ, Turville C, Ye H (2019) Projections of southern hemisphere tropical cyclone track density using CMIP5 models. Clim Dyn 52:6065–6079. https://doi.org/10.1007/s00382-018-4497-4

Bougeault P, Lacarrèr P (1989) Parameterization of orography-induced turbulence in a mesobeta—scale model. Mon Wea Rev 117:1872–1890. https://doi.org/10.1175/1520-0493(1989)117<1872:POOITI>2.0.CO;2

Chen F, Dudhia J (2001) Coupling an advanced land surface-hydrology model with the Penn State-NCAR MM5 modeling system. Part I: model implementation and sensitivity. Mon Wea Rev 129:569–585. https://doi.org/10.1175/1520-0493(2001)129<0569:CAALSH>2.0.CO;2

Durrant T, Greenslade D, Hemer M, Trenham C (2014) A global wave hindcast focused on the Central and South Pacific. The Centre for Australian Weather and Climate Research Technical Report No. 070. ISSN: 1835-9884

European network for earth system modeling (2019) CMIP5 models and grid resolution. https://portal.enes.org/data/enes-model-data/cmip5/resolution. Accessed 25 Jul 2019.

Flato G, Marotzke J, Abiodun B, Braconnot P, Chou SC, Collins W, Cox P, Driouech F, Emori S, Eyring V, Forest C, Gleckler P, Guilyardi E, Jakob C, Kattsov V, Reason C, Rummukainen M (2013) Evaluation of climate models. In: Climate Change 2013: The Physical Science Basis. Contribution of Working Group I to the Fifth Assessment Report of the Intergovernmental Panel on Climate Change. Cambridge University Press, Cambridge, United Kingdom and New York

Hemer MA, Katzfey J, Trenham CE (2013) Global dynamical projections of surface ocean wave climate for a future high green gas emission scenario. Ocean Model 70:221–245

Hemer MA, Trenham CE (2016) Evaluation of a CMIP5 derived dynamical global wind wave climate model ensemble. Ocean Model 103:190–203

Hill KA, Lackmann GM (2011) The impact of future climate change on TC intensity and structure: A downscaling approach. J Clim 24:4644–4661. https://doi.org/10.1175/2011JCLI3761.1

Hoffman RN, Kalnay E (1983) Lagged average forecasting, an alternative to Monte Carlo forecasting. Tellus Ser A 35:110–118. https://doi.org/10.1111/j.1600-0870.1983.tb00189.x

Hong SY, Lim J-OJ (2006) The WRF single moment 6-class microphysics scheme (WSM6). J Korean Meteor Soc 42:129–151

Iacono MJ, Delamere JS, Mlawer EJ, Shephard MW, Clough SA, Collins W (2008) Relative forcing by long-lived greenhouse gases: calculation with the AER radiative transfer models. J Geophys Res Atmos 113:D13102. https://doi.org/10.1029/2008JD009944

Jiménez PA, Dudhia J, González-Rouco JF, Navarro J, Montávez JP, García-Bustamante E (2012) A revised scheme for the WRF surface layer formulation. Mon Wea Rev 140:898–918. https://doi.org/10.1175/MWR-D-11-00056.1

Kain JS (2004) The Kain-Fritsch convective parameterization: an update. J App Meteolol 43:170-181. doi:.1175/1520-0450(2004)043<0170:TKCPAU>2.0.CO;2.

Kanada S, Takemi T, Kato M, Yamasaki S, Fudeyasu H, Tsuboki K, Arakawa O, Takayabu I (2017a) A multimodel intercomparison of an intense typhoon in future, warmer climate by four 5-km-mesh models. J Clim 30:6017–6036. https://doi.org/10.1175/JCLI-D-16-0715.1

Kanada S, Tsujino S, Aiki H, Yoshioka MK, Miyazawa Y, Tsuboki K, Takayabu I (2017b) Impacts of SST patterns on rapid intensification of typhoon Megi (2010). J Geophys Res Atmos 122:13245–13262. https://doi.org/10.1002/2017JD027252

Knutson TR, McBride JL, Chan J, Emanuel K, Holland G, Landsea C, Held I, Kossin JP, Srivastava AK, Sugi M (2010) Tropical cyclones and climate change. Nature Geosci 3:157–163. https://doi.org/10.1038/NGEO.779

Lackmann GM (2015) Hurricane Sandy before 1900 and after 2100. Bull Amer Meteor Soc 96:547–560. https://doi.org/10.1175/BAMS-D-14-00123.1

Laugel A, Menendez M, Benoit M, Mattarolo G, Méndez F (2014) Wave climate projections along the French coastline: Dynamical versus statistical downscaling. Ocean Model 84:35–50

Marciano CG, Lackmann GM, Robinson WA (2015) Changes in U.S. East coast cyclone dynamics with climate change. J Clim 28:468–484. https://doi.org/10.1175/JCLI-D-14-00418.1

Martínez-Asensio A, Tsimplis MN, Marcos M, Feng X, Gomis D, Jordà G, Josey SA (2016) Response of the North Atlantic wave climate to atmospheric modes of variability. Int J Clim 36:1210-1225. https://doi.org/10.1002/joc.4415.

Meredith EP, Semenov VA, Maraun D, Park W, Chernokulsky V (2015) Crucial role of Black Sea warming in amplifying the 2012 Krymsk precipitation extreme. Nat Geosci 8:615–619. https://doi.org/10.1038/ngeo2483

Mori N, Shimura T, Yasuda T, Mase H (2013) Multi-model climate projections of ocean surface variables under different climate scenarios—Future change of waves, sea level and wind. Ocean Eng 71:122–129

Nakamura R, Shibayama T, Esteban M, Iwamoto T (2016) Future typhoon and storm surges under different global warming scenarios: case study of typhoon Haiyan (2013). Nat Hazards 82:1645–1681. https://doi.org/10.1007/s11069-016-2259-3

Nasuno T, Yamada H, Nakano M, Kubota H, Sawada M, Yoshida R (2016) Global cloud-permitting simulations of Typhoon Fengshen (2008). Geosci Lett 3:32. https://doi.org/10.1186/s40562-016-0064-1

National Centers for Environmental Prediction (NCEP)/National Weather Service/NOAA/U.S. Department of Commerce (2015) NCEP GDAS/FNL 0.25 Degree Global Tropospheric Analyses and Forecast Grids. doi:10.5065/D65Q4T4Z. Research Data Archive at the National Center for Atmospheric Research, Computational and Information Systems Laboratory, Boulder, Colo. (Updated daily.) Accessed 02 DEC 2018.

Nayak S, Takemi T (2019) Dynamical downscaling of Typhoon Lionrock (2016) for assessing the resulting hazards under global warming. J Meteorol Soc Japan 97:69–88

Oku Y, Takemi T, Ishikawa H, Kanada S, Nakano M (2010) Representation of extreme weather during a typhoon landfall in regional meteorological simulations: a model intercompasiron study for Typhoon Songda (2004). Hydrol Res Lett 4:1–5. https://doi.org/10.3178/HRL.4.1

Patricola CM, Wehner MF (2018) Anthropogenic influence on major tropical cyclone events. Nature. 563:339–346. https://doi.org/10.1038/s41586-018-0673-2

Reynolds RW, Smith TM, Liu C, Chelton DB, Casey KS, Schlax MG (2007) Daily high-resolution-blended analyses for sea surface temperature. J Clim 20:5473–5496. https://doi.org/10.1175/2007JCLI1824.1

Sato T, Kimura F, Kitoh A (2007) Projection of global warming onto regional precipitation over Mongolia using a regional climate model. J Hydrol 333:144–154

Schär C, Frei C, Lüthi D, Davies HC (1996) Surrogate climate-change scenarios for regional climate models. Geophys Res Lett 23:669–672. https://doi.org/10.1029/96GL00265
Shibata A (2006) A wind speed retrieval algorithm by combining 6 and 10 GHz data from Advanced Microwave Scanning Radiometer: Wind speed inside hurricanes. J Oceanogr 62:351–359
Shimura T, Mori N, Mase H (2015) Future projection of ocean wave climate: Analysis of SST impacts on wave climate change in the western North Pacific. J Clim 28:3171–3190
Skamarock WC, Klemp JB, Dudhia J, Gill DO, Barker JM, Duda MG, Huang X-Y, Wang W, Powers JG (2008) A description of the advanced research WRF version 3. NCAR Technical Note, NCAR/RN-475+STR. https://doi.org/10.5065/D68S4MVH
Takayabu I, Hibino K, Sasaki H, Shiogama H, Mori N, Shibutani Y, Takemi T (2015) Climate change effects on the worst-case storm surge: a case study of Typhoon Haiyan. Environ Res Lett 10:064011. https://doi.org/10.1088/1748-9326/10/8/089502
Taniguchi K (2018) A simple ensemble simulation technique for assessment of future variations in specific high-impact weather events. J Geophys Res: Atmos 123:3443–3461
Taniguchi K, Sho K (2015) Application of the pseudo global warming dynamic downscaling method to the Tokai Heavy Rain in 2000. J Meteor Soc Japan 93:551–570. https://doi.org/10.2151/jmsj.2015-043
Tasnim KM, Shibayama T, Esteban M, Takagi H, Ohira K, Nakamura R (2015) Field observation and numerical simulation of past and future storm surges in the Bay of Bengal: case study of cyclone Nargis. Nat Hazards 75:1619–1647
Taylor KE, Stouffer RJ, Meehl GA (2012) An overview of CMIP5 and the experiment design. Bull Amer Meteor Soc 93:485–498
Timmermans B, Stone D, Wehner M, Krishnan H (2017) Impact of tropical cyclones on modeled extreme wind-wave climate. Geophys Res Lett 44:1393–1401. https://doi.org/10.1002/2016GL071681
Tolman HL (2009) User manual and system documentation of WaveWatch III version 3.14, Technical Note 276, NOAA/NWS/NCEP/MMAB.
Tolman HL, Chalikov D (1996) Source terms in a third-generation wind wave model. J Phys Oceanography 26:2497–2518. https://doi.org/10.1175/1520-0485(1996)026<2497:STIATG>2.0.CO;2
Walsh KJE, McBride JL, Klotzbach PJ, Balachandran S, Camargo SJ, Holland G, Knutson TR, Kossin JP, Lee T, Sobel A, Sugi M (2015) Tropical cyclones and climate change. WIREs Clim Change. https://doi.org/10.1002/wcc.371
Walsh KJE, McInnes KL, McBride JL (2012) Climate change impacts on tropical cyclones and extreme sea levels in the South Pacific—a regional assessment. Glob Planet Change 80-81:149–164. https://doi.org/10.1016/j.gloplacha.2011.10.006
Yoshida K, Sugi M, Mizuta R, Murakami H, Ishii M (2017) Future changes in tropical cyclone activity in high-resolution large-ensemble simulations. Geophys Res Lett 44:9910–9917. https://doi.org/10.1002/2017GL075058
Zhang C, Wang Y (2017) Projected future changes of tropical cyclone activity over the Western North and South Pacific in a 20-km-mesh regional climate model. J Clim 30:5923–5941. https://doi.org/10.1175/JCLI-D-16-0597.1

Publisher's Note